The Relationship between Pre-landfall Intensity Change and Post-landfall Weakening of Tropical Cyclones over China

Wenjun Han[a,b], Yuqing Wang[c*], and Lu Liu[a]

[a] *State Key Laboratory of Severe Weather, Chinese Academy of Meteorological Sciences, China Meteorological Administration, Beijing, China*

[b] *College of Earth and Planetary Sciences, University of Chinese Academy of Sciences, Beijing, China*

[c] *International Pacific Research Center and Department of Atmospheric Sciences, School of Ocean and Earth Science and Technology, University of Hawaii at Manoa, Honolulu, HI, USA*

October 28, 2022 (submitted)

November 30, 2022 (revised)

Dateline

Submitted to ***Frontiers in Earth Science***

* *Corresponding author*: Yuqing Wang, yuqing@hawaii.edu

Abstract

The accurate prediction of the weakening of landfalling tropical cyclones (TC) is of great importance to the disaster prevention but is still challenging. In this study, based on the 6-hourly TC best-track data and global reanalysis data, the relationship between the intensity change prior to landfall of TCs and the energy dissipation rate after landfall over mainland China is statistically analyzed, and the difference between East and South China is compared. Results show that TCs making landfall over East China often experienced pre-landfall weakening and usually corresponded to a rapid decay after landfall, while most TCs making landfall over South China intensified prior to landfall and weakened slowly after landfall. The key factors affecting both pre-landfall intensity change and post-landfall energy dissipation rate are quantitatively analyzed. It is found that the decreasing sea surface temperature (SST), increasing SST gradient, and increasing environmental vertical wind shear are the major factors favoring high pre-landfall weakening occurrence, leading to rapid TC weakening after landfall over East China. In South China, changes in the large-scale environmental factors are relatively small and contribute little to the post-landfall weakening rate.

Keywords: landfalling tropical cyclones, intensity change, post-landfall weakening rate, large-scale environmental factors

1. Introduction

Landfalling tropical cyclones (LTCs), especially those weakening slowly after landfall, seriously threaten to our life and property (Klotzbach et al., 2018). LTCs caused annual deaths of 472 and annual economic loss of 28.7 billion RMB in China during 1983-2006 (Zhang et al., 2009). Typhoon Nina (7503) triggered a disastrous dam collapse in the inland province of Henan in 1975, which led to flood spread to more than 1 million hectares of farmland in 29 counties and cities and eventually caused a total economic loss of about 10 billion RMB (Liu et al., 2009). Therefore, it is important but challenging for accurate prediction of LTC intensity and thus for disaster prevention because of dramatically changes in tropical cyclone (TC) structure and intensity (Elsberry and Tsai, 2014). From a social and economic point of view, it is also very important to accurately predict the regional changes in the intensity of LTCs (Walsh et al., 2016).

The weakening of TCs after landfall is driven by many factors, including LTC intensity (Tuleya et al., 1984), land-atmosphere interaction (Andersen et al., 2013, 2014), and topographic effect (Done et al., 2020). The sudden reduction of surface enthalpy source and the increase of surface roughness would lead to weakening of the eyewall convection and the decrease of surface wind speed, and thus the filling of a TC over land (Miller, 1964; Power, 1991; Ooyama, 1969; Tuleya, 1994). Li et al. (2020) statistically analyzed the TCs making landfall over the North Atlantic in recent fifty years and found that the increasing sea surface temperature (SST) increases the moisture stored in TCs during its passage over the coastal ocean, which can supply extra enthalpy source and help maintain warm-core structure and thus the intensity of TCs after landfall. However, some other studies have found that the SST may not be a major factor determining the weakening rate of LTCs over the western North Pacific (Chen et al., 2021). In addition, the influence of large-scale environmental conditions on LTC weakening cannot be ignored. Wood and Ritchie (2015) studied the rapid weakening events of TCs in the North Atlantic and eastern North Pacific during 1982–2013. Their results showed that the strong SST gradient and the contribution by dry air intrusion induced more rapid weakening events in the eastern North Pacific than in the North Atlantic. The increase in coastal SST, land surface temperature and soil moisture, the decrease in low-level vertical wind shear (VWS), and the increase in upper-level divergence are all favorable for intensification of TCs and their survival after landfall (Wang et al., 2015; Liang et al., 2016; Liu et al., 2020; Ji et al., 2020). Previous studies have qualitatively examined how environmental factors affect the weakening of TCs while a quantitative study on the environmental factors affecting the weakening of TCs after landfall has not been comprehended.

In recent years, more attention has been given to how nearshore intensity change of TCs may affect the post-landfall weakening. TCs that experienced rapid intensification prior to landfall are more destructive, such as Hurricanes Andrew (1992), Opal (1995), and Charley (2004), all resulted in devastating to the coastal regions in the United States (Franklin et al., 2006). Rappaport et al. (2010) discussed the intensity change of TCs within 48 h before landfall along the Gulf coast and concluded that weak (intense) TCs strengthened (weakened) prior to landfall. Park et al. (2011) analyzed TCs making landfall in Korea and Japan and found a trend of increasing duration after landfall relative to the intensity prior to landfall, and further affect the temporal variation of the TC-induced rainfall in the region. Zhu et al. (2021) found that hurricanes undergoing rapid intensification prior to landfall weakened at a slower rate after landfall in the Continental United States and the weakening rate was also weakly and positively correlated with the landfall intensity. They also indicated that the pre-landfall intensification was more common along the Gulf Coast but there was no significant correlation between regions and weakening rate. Song et al (2021) further showed that a slower weakening rate prior to landfall of TCs over the South China Sea and an increased intensification rate prior to landfall of TCs east of the Philippines had a significant linkage to warmer ocean and greater upper-level divergence.

The aforementioned studies have mainly focused on either the TC pre-landfall intensity change or regional distribution of weakening rate after landfall. In particular, few studies have involved whether the post-landfall weakening rate of LTCs over China exhibits any obvious regional characteristics related to the pre-landfall intensity change (Kruk et al., 2010; Zhu et al., 2021). Furthermore, it is still unclear how oceanic and atmospheric environmental factors regulate the relationship between the pre-landfall intensity change and the post-landfall weakening of TCs. The main objectives of this study are 1) to explore the intensity change characteristics of LTCs prior to landfall over China, 2) to analyze the difference in the weakening rate of TCs over South China and East China, 3) to identify key factors affecting LTC dissipation and quantify their relative contributions based on the box difference index (BDI) method. The rest of the paper is organized as follows. Section 2 describes the data and analysis methods used in this study. The intensity change of TCs prior to landfall over China and the weakening of TCs after landfall are presented in section 3. Section 4 shows the spatial distribution characteristics of LTCs. The relative importance of various factors affecting the decay and regional differences is analyzed and discussed in section 5. The main findings are summarized in the last section.

2. Data and methods

a. Data

The 6-hourly TC best-track data used in this study were obtained from the China Meteorological Administration-Shanghai Typhoon Institute (CMA/STI), which include 6-hourly TC center location (longitude and latitude), maximum sustained (2-min mean) near-surface wind speed (V_{max}) and minimum central sea level pressure (Ying et al., 2014). The 6-hourly best track data were linearly interpolated to hourly data (Liu et al., 2021) for the subsequent calculations of the accumulated cyclone energy (ACE), the change rate of V_{max}, and landfalling dissipation rate (LFDR).

We have focused on TCs whose centers crossed the coastline of mainland China (except Taiwan Island) at least once during their lifetimes. We first checked the hourly data to determine whether a TC was on land and then calculated the intersection of the line between 6-h pre-landfall and 6-h post-landfall using the coastline to determine the TC landfalling location and intensity (Hu et al., 2017). We only considered the landfall location south of 40°N in the peak TC season from June to October (Wang et al., 2015) during 1979–2018. In total, 90 TCs cases including at least three continuous 6-h records prior to and after landfall were selected in our study.

The environmental data were acquired from the European Centre for Medium-Range Weather

Forecasts (ECMWF) interim reanalysis (ERA-Interim) data at the horizontal resolution of 0.75°×0.75°, including the horizontal winds, vertical *p*-velocity, and specific humidity (Dee et al., 2011). The filtering algorithm of Kurihara et al. (1993) was used to remove the disturbance field, including the TC vortex, with the wavelengths less than 1,000 km from the unfiltered large-scale environmental fields at a given time. The filtered data were used to calculate the environmental vorticity, divergence, vertical wind shear (between 1000–300-hPa and 700–300-hPa, respectively), and water vapor flux divergence (QVDIV) (Table 1), in our analyses on environmental effect on TC intensity change during landfall.

b. Methods

The average change rate in sustained near-surface wind speed V_{max} (r_{vmax}) is introduced as an index to characterize a TC that is intensifying or weakening within 18 h prior to landfall following Zhu et al. (2021):

$$r_{vmax} = \frac{V_{max,t} - V_{max,t-18}}{18h}$$

where $V_{max,t}$ and $V_{max,t-18}$ represent the sustained near-surface wind speed at the time of landfall and the time of 18 hours prior to landfall. The intensifying TCs and weakening TCs are bounded by the 90th percentiles of positive values and negative values of r_{vmax}, respectively, and the remaining are considered as neutral TCs. Finally, 25 intensifying cases, 41 weakening cases, and 24 neutral cases were identified in our following analyses. Note that we used the period of 18 hours instead of 24 hours used in Zhu et al. (2021) because most TCs that made landfall over China weakened to tropical depression about 18 hours after landfall. We also examined the 24 h period with the results quite similar to those obtained using 18 hours discussed herein.

Accumulated cyclone energy (ACE) is a metric to express the energy released by a TC during its lifetime (Bell et al., 2000; Trenberth et al., 2005; Emanual, 2005). We used hourly interpolated data to compute the pre-landfall ACE (ACE_{-18h}) and post-landfall ACE (ACE_{+18h}) of a TC during its landfalling period (Vitat, 2009; Truchelut, 2007):

$$\mathrm{ACE} = 10^{-4} \sum V_{max}^2$$

where V_{max} is sustained near-surface wind speed with four continuous 6 hourly records prior to (-18h, -12h, -6h, 0h) or after (0h, 6h, 12h, 18h) landfall. The index is scaled by 10^{-4} to make them more manageable.

In addition to quantifying the post-landfall weakening of TCs, Zhu et al. (2021) also defined the landfalling dissipation rate (LFDR) given below:

$$\mathrm{LFDR} = 1 - \frac{\mathrm{ACE}_{+18\mathrm{h}}}{\mathrm{ACE}_{-18\mathrm{h}}}$$

A TC with higher $\mathrm{ACE}_{-18\mathrm{h}}$ and lower $\mathrm{ACE}_{+18\mathrm{h}}$ has greater LFDR, which means that the TC weakens more rapidly because of the larger energy dissipation.

A box difference index (BDI) was used to quantitatively measure the difference of key factors in intensifying (weakening) TCs compared to neutral TCs (Fu et al., 2012; Li et al., 2020):

$$\mathrm{BDI_{ITC}} = \frac{\mathrm{M_{ITC}} - \mathrm{M_{NTC}}}{\sigma_{\mathrm{ITC}} - \sigma_{\mathrm{NTC}}};\ \mathrm{BDI_{WTC}} = \frac{\mathrm{M_{WTC}} - \mathrm{M_{NTC}}}{\sigma_{\mathrm{WTC}} - \sigma_{\mathrm{NTC}}}$$

where $\mathrm{M_{ITC}}$ and σ_{ITC} ($\mathrm{M_{WTC}}$ and σ_{WTC}, $\mathrm{M_{NTC}}$ and σ_{NTC}) represent the mean and standard deviation of the variables for the intensifying (weakening, neutral) TC cases within 18 hours prior to landfall. The BDI is a number between -1.0 and 1.0. If the absolute value of index is greater, the corresponding factor is easier to trigger the intensifying (or weakening) process.

3. Post-landfall weakening of TCs in the three categories

Figure 1 shows the intensity change characteristics of TCs in, respectively, the intensifying, weakening, and neutral categories during landfall. To compare the intensity evolution during landfall, we defined the ratio of the maximum near-surface wind speed (V_{max}) to that at the time of landfall (V_{0max}), which can also be termed relative intensity (V_{max}/V_{0max}). The ratios in all weakening cases are greater than 1.0 because the TC intensity decreases with time prior to landfall while those in intensifying TCs are less than 1.0 except for in a few intensifying cases whose ratios are still greater than 1 because their maximum intensities appeared at 6 h prior to landfall (Figure 1a), indicating that the weakening started 6 hours prior to landfall rather than at the time of landfall. The mixed distribution pattern of TC cases after landfall illustrates that some individual TCs weakened rapidly while some others weakened slowly or a few even maintained. The pre- and post-landfall ACE distributions are compared in Figure 1b. The weakening TCs with an average ACE of 1.75×10^4 m^2 s^{-2} possess more energy prior to landfall but less energy after landfall relative to that at the time of landfall. This means that the weakening cases prior to landfall would experience greater energy dissipation after landfall. For intensifying TCs, the post-landfall ACE decreased slowly or even maintained their intensities. The time evolutions of the average V_{max} and the average 6-h intensity change from -18 h to +18 h in the three categories are compared in Figures 1c and 1d, respectively. The average V_{max} of intensifying TCs increased from -18 h to -6 h and then decreased toward landfall while that of weakening TCs decreased during the whole landfalling process. The average V_{max} after landfall in weakening TCs is less than that in intensifying TCs. From the 6-h intensity decay rate, we can see that the intensification rate of the pre-landfall intensifying TCs decreases and the weakening rate of the pre-landfall weakening TCs increases prior to landfall. Both types of the TCs weaken rapidly within 6 h after landfall and then the weakening rate shows a decreasing trend.

To explore whether the pre-landfall intensity change has a direct relationship with the post-landfall intensity decay, we first examined the correlation between ACE_{-18h} and ACE_{+18h} and found that they are highly correlated, which is statistically significant over the 99% confidence level (Figures 2a~2c). Namely, a strong TC that undergoes slow weakening prior to landfall possesses relatively higher intensity at landfall and tends to decay more rapidly after landfall, while a weak TC with lower ACE prior to landfall decays more slowly after landfall. This is different from those documented in Zhu et al. (2021), who found that the correlation for the weakening TCs is very weak and insignificant. The difference may be due to the different environmental conditions in the United States and mainland China.

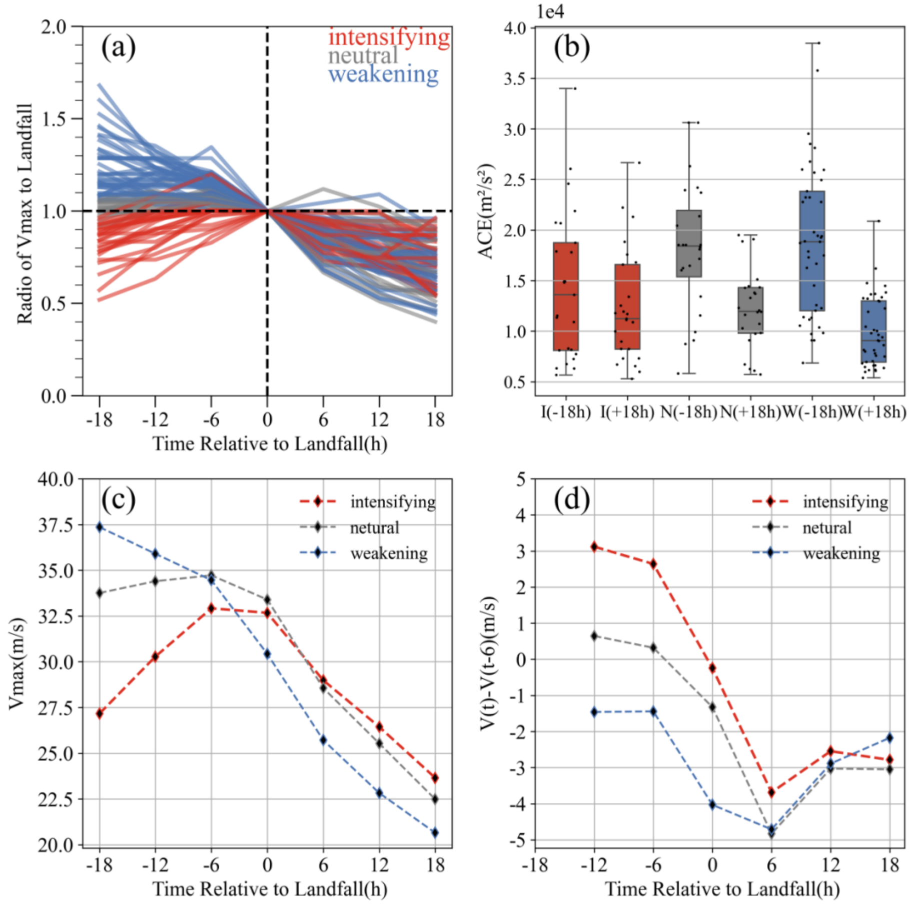

Figure 1. (a) Time evolutions of the ratio of maximum sustained near-surface wind to that at the time of landfall (V_{max}/V_{0max}); (b) the accumulated cyclone energy (ACE) within 18 h prior to landfall (-18 h) and 18 h after landfall (+18 h), with black dots representing the TC cases and the horizontal line representing the median; (c) the average V_{max} from -18 h to +18 h during landfall; and (d) the average 6-h intensity change. The red, gray and blue colors represent intensifying, neutral and weakening TCs, respectively.

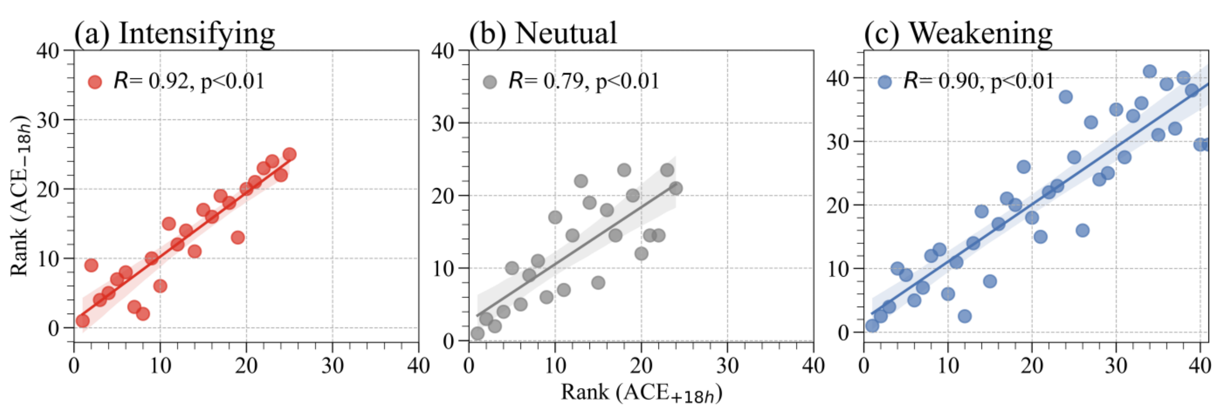

Figure 2. Mann-Kendall's tau-b correlation (non-parametric) of the rank between accumulated cyclone energy (ACE) within 18 h prior to landfall (-18h) and 18 h after landfall (+18h) for (a) intensifying, (b) neutral, and (c) weakening TCs.

We further choose LFDR as a metric to describe the energy dissipation process during landfall, which can help quantify the influence of pre-landfall intensity on the subsequent post-landfall dissipation. As we can see from Figure 3a, r_{vmax} has a significant negative correlation with LFDR with a correlation coefficient as high as -0.6, which is statistically significant over the 99% confidence level. This indicates that a TC undergoing pre-landfall intensification would be filled slowly after landfall while a TC that weakens prior to landfall would dissipate rapidly, which is consistent with the results for hurricanes making landfall over the United States reported by Zhu et al. (2020). Previous studies have also demonstrated that the landfall intensity is one of the factors related to the weakening characteristics of TCs after landfall. Li et al. (2017) found that increasing landfall intensity would result in greater destruction over China. However, recent studies have revealed that TCs with higher landfall intensity usually have longer duration after landfall (Liu et al., 2020; Liu et al., 2021; Song et al., 2021; Chen et al., 2021). This does not necessarily mean that the weakening of a strong TC is slower. We found that the LFDR is significantly correlated with the landfall intensity over the 95% confidence level (Figure 3b). Since r_{vmax} depends on landfall intensity (Figure 3c), we can conclude that the landfall intensity also has a weak effect on the post-landfall weakening.

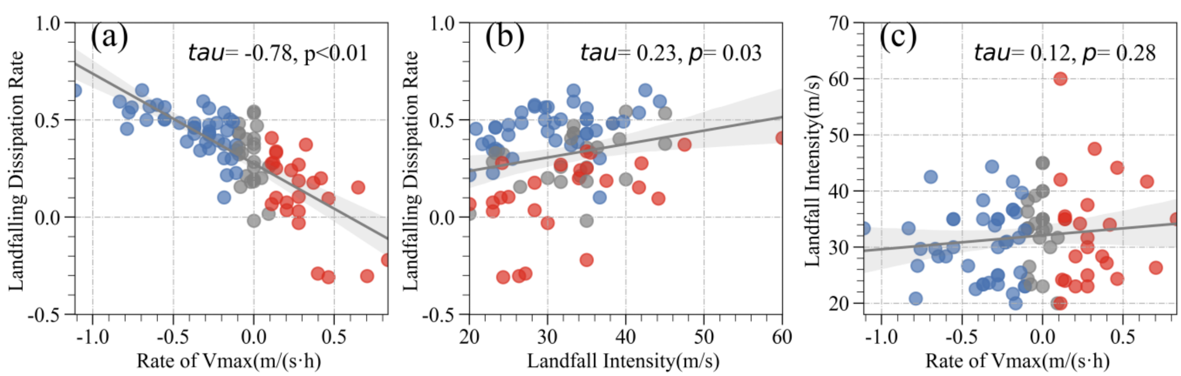

Figure 3. (a) The relationship between the rate of V_{max} (r_{vmax}) and landfalling dissipation rate (LFDR) in intensifying (red), neutral (gray) and weakening (blue) TCs. Solid line represents the linear regression trend. Dashed lines show the 99% confidence interval. (b) As in (a) but for landfall intensity (V0max) and LFDR. (c) As in (a) but for r_{vmax} and landfall intensity.

4. Characteristics of spatial distribution

Figure 4 depicts the spatial distribution of the relative intensity (V_{max}/V_{0max}) for TCs in the three individual categories and for all TCs as a whole. The relative intensity of TCs making landfall in northern Taiwan Island and East China Sea shows a maximum and decreases toward the north (Figure 4d), which is dominated by the weakening TCs (Figure 4c). However, the pre-landfall relative intensity in the South China Sea shows little change. This is mainly because of the high landfall frequency over the South China Sea (Liu et al., 2020), dominated by both northwestward moving intensifying TCs (Figure 4a) and westward moving weakening TCs (Figure 4c).

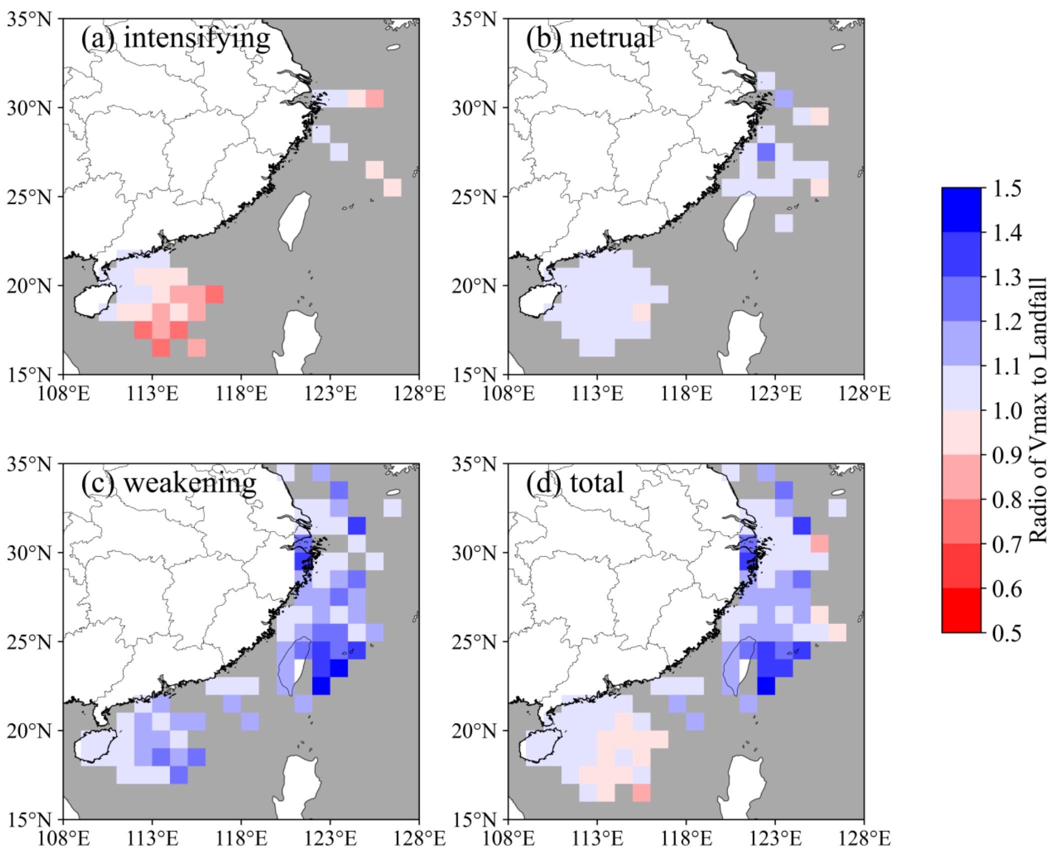

Figure 4. Spatial distribution of relative intensity (V_{max}/V_{0max}) for (a) intensifying, (b) neutral, (c) weakening, and (d) total TCs prior to landfall.

We next examine the spatial distribution of the relationship between pre-landfall TC intensity change (r_{vmax}) and the inland LFDR, with the results shown in Figure 5. Most frequent landfalls of TCs occurred in the southeastern Hainan Island, which are classified into South China in our study, and the northern Fujian Province and Zhejiang Province (namely East China). Due to the blocking effect of the Central Range over the Taiwan Island, TCs making landfall in Guangdong and southern Fujian often decayed too quickly to maintain over 18 h, which were not included in our analysis. As we can see from Figure 5a, the intensifying TCs with larger r_{vmax} were distributed in South China. Only two cases are located in the northern Zhejiang, namely Bill (8807) in 1988 and YAGI (1814) in 2018 because of the sufficient water vapor supply to support active convection in the inner core of the TCs (Jiang et al., 1989; Huang et al., 2018; Ji et al., 2019). The weakening TCs were densely distributed over East China (Figure 5c), and neutral TCs were distributed in both South and East China (Figure 5b). This indicates that TCs making landfall in East China would carry larger pre-landfall ACE and tend to have greater landfall intensity.

We now discuss the spatial distribution of inland LFDR in East and South China. Intensifying TCs in South China show weak LFDR, with values ranging from -0.2 to 0.45. Note that a few weakening TCs with small LFDR also made landfall in this area, making the dissipation pattern a little bit complicated there. The larger LFDR ranging from 0.45 to 0.60 appeared in East China, all of which came from the weakening TCs. This indicates that the pre-landfall weakening TCs in East China experienced rapid dissipation after landfall. Some previous studies have shown that the apparent regional difference over mainland China might be controlled by various large-scale environmental conditions (Wong et al., 2008; Song et al., 2021). Whether the large-scale environmental factors affect r_{vmax} and LFDR will be discussed in detail in the next section.

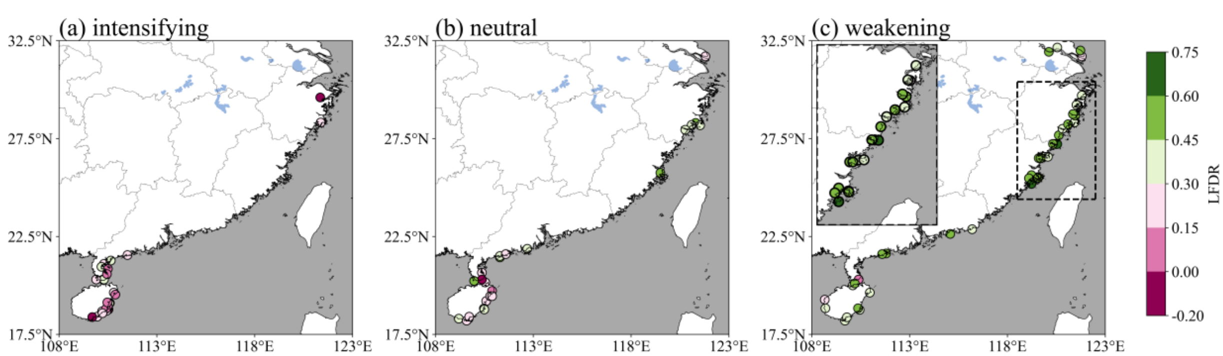

Figure 5. Spatial distribution of landfalling dissipation rate (LFDR) for (a) intensifying, (b) neutral, (c) weakening TCs. The weakening TCs over East China is magnified in the inset box for clarity in (c).

5. Factors affecting LFDR over South China and East China

Most studies have shown that the rapid weakening of TCs may be caused by low SST and large SST gradient (Zhang et al., 2007; Qian and Zhang, 2013; DeMaria et al., 2012; Wood and Ritchie, 2015) and large-scale environmental factors, such as strong vertical wind shear and dry air intrusion (Frank and Ritchie, 2001; Wood and Ritchie, 2015; Wang et al., 2015; Fei et al., 2019). In our study, we selected SST, SST gradient, environmental low-level vorticity, upper-level divergence, vertical wind shear, mid-level specific humidity, and low-level water vapor flux divergence as possible environmental factors affecting LFDR after landfall over mainland China and compare the different characteristics of persistence of these factors in South China and East China (Table 1).

Table 1. The factors analyzed in this study with their units and descriptions given.

Factors	Unit	Description
SST	°C	Sea surface temperature within a radius of 3 degrees of the TC center
SST Gradient	°C km^{-1}	SST gradient within a radius of 3 degrees of the TC center
VOR850	s^{-1}	Environmental relative vorticity averaged within a radius of 9 degrees of the TC center at 850 hPa
DIV200	s^{-1}	Environmental divergence averaged within a radius of 9 degrees of the TC center at 200 hPa
VWS300-1000	m s^{-1}	Environmental vertical wind shear averaged within a radius of 4.5 degrees of the TC center between 1000 hPa and 300 hPa
UVWS300-1000	m s^{-1}	Zonal environmental vertical wind shear averaged within a radius of 4.5 degrees of the TC center between 1000 hPa and 300 hPa
VWS700-1000	m s^{-1}	As in VWS300-1000 but between 1000 hPa and 700 hPa
UVWS700-1000	m s^{-1}	As in UVWS300-1000 but between 1000 hPa and 700 hPa
q500	g kg^{-1}	Environmental specific humidity averaged within a radius of 5 degrees of the TC center at 500 hPa
QVDIV	s^{-1}	Environmental water vapor flux divergence within a radius of 9 degrees of the TC center between 1000 hPa and 850 hPa

Table 2 compares the linear correlation coefficients between the change and average value of each of the pre-landfall factors and LFDR. Among them, SST, SST gradient, zonal deep vertical wind shear (UVWS), and low-level water vapor flux divergence (QVDIV) are highly correlated with LFDR, while upper-level divergence (DIV200) and mid-level specific humidity (q500) show weak correlations with LFDR, while low-level vorticity has no obvious correlation with LFDR.

We can see that the average SST was 28.47°C with the negative correlation coefficient of -0.28 with LFDR. Compared with 18 h prior to landfall, the SST decreased by 0.44°C at the time of landfall with a negative correlation of -0.31 with LFDR. This implies that a TC crossing a region with lower SST and greater decreasing SST trend has a larger LFDR. This is consistent with previous result in Li et al. (2020), who drawn a conclusion that the water content carried by a hurricane would be reduced to retard the supply of ocean heat when the nearshore SST was cooler and decreased faster. However, Bender et al. (1993) showed that the upwelling and vertical mixing under a TC had a negative effect on TC intensity and could lead to rapid TC weakening after landfall. In addition to SST, the SST gradient is another key ocean parameter. Prior to landfall, the average SST gradient was 3.67×10^{-3} °C km^{-1} and increased by 1.25×10^{-3} °C km^{-1}with the significant positive correlation with LFDR, which implies that the large SST gradient favors rapid decay of TC after landfall.

Table 2. The average factors and Mann-Kendall correlation coefficients with LFDR. Change (T_{0h} -T_{-18h}), average values indicate the pre-landfall change and average value, respectively. Correlation coefficients that are statistically significant above 95% confidence level are boldfaced.

Factors	Change Values		Average Values	
	Change.	Corr coef.	Avg.	Corr coef.
SST	-0.44	**-0.31**	28.47	**-0.28**
SST Gradient	1.25×10^{-3}	**0.20**	3.67×10^{-3}	**0.26**
VOR850	0.06×10^{-7}	-0.04	-0.96×10^{-6}	0.11
DIV200	-0.60×10^{-6}	-0.04	-0.12×10^{-5}	**-0.22**
VWS300-1000	0.31	**0.14**	4.88	**0.19**
UVWS300-1000	0.92	**0.22**	-2.19 m s^{-1}	**0.23**
VWS700-1000	0.38	-0.01	1.78 m s^{-1}	0.05
UVWS700-1000	0.10	0.09	-0.34 m s^{-1}	0.01
q500	0.067	**-0.19**	4.08	-0.03
QVDIV	0.045×10^{-6}	0.01	-0.06×10^{-6}	**0.25**

The large-scale environmental atmospheric conditions are also important to TC intensity change and thus the weakening of LTCs. From Table 2, we can see that the low-level vorticity shows little correlation with LFDR, while the upper-level divergence is negatively correlated with LFDR. This suggests that the upper tropospheric convergence forcing (-0.12×10^{-5} s^{-1}) may contribute to the weakening of TCs after landfall over China. The VWS is considered a detrimental dynamical environmental factor that is unfavorable for TC intensification (Zeng et al., 2010; Liang et al., 2016; Wang et al., 2015). We examined both the deep-layer VWS between 300–1000 hPa and the low-level VWS between 700–1000 hPa, representative of the VWS effect on TC intensity change over the western North Pacific (Wang et al., 2015). As we can see from Table 2, the deep-layer VWS and the deep-layer vertical shear of zonal wind have higher linear correlations with LFDR (r=0.19 and 0.23, respectively) than the low-level VWS, which implies that TCs with larger VWS may weaken more rapidly after landfall over China. This is different from the results of Wang et al. (2015), who found the low-level VWS during the active TC season is more significantly correlated with TC intensity change than the VWS at other layers. This is mainly because they considered the area of 123°E–180°E while we focused on the area west of 127°E. Importantly, the vertical shear of zonal wind can have a more detrimental effect on TC intensity after landfall, or equivalently more beneficial to LFDR. This suggests that the effect of VWS on TC intensity depends not only on the magnitude of the shear but also on the direction of the shear. For example, Wang et al. (2013) found that nearly 70% of the rapid intensification of TCs occurred in easterly shear while westerly shear inhibits TC development, suggesting that westerly shear has a greater negative effect on TC intensity than easterly shear.

The dry air intrusion and water vapor supply are two other factors that may affect the weakening rate of landfalling TCs (Wood and Ritchie, 2015; Fei et al., 2019). We thus examined the mid-level environmental specific humidity and low-level water vapor flux divergence. The change in 500-hPa specific humidity prior to landfall shows a weakly negative correlation with the LFDR, with the correlation coefficient of -0.19, indicating that the TCs experiencing large decreasing specific humidity nearshore usually tend to weaken rapidly after landfall. Note that the specific humidity decreased little prior to landfall with one possible reason is that changes in the environmental humidity in South China and East China offset each other, which will be discussed later (Figure 6g). The water vapor flux divergence prior to landfall is positively correlated with LFDR, with the correlation coefficient of 0.25, which is statistically significant above 95%

confidence level, indicating that the reduced moisture supply with weak horizontal water vapor flux convergence provides favorable environmental conditions for TC post-landfall weakening.

Based on the above correlation analysis, we examine the trends of key factors, including SST, SST gradient, DIV200, VWS300-1000, UVWS300-1000, q500, and QVDIV during landfall over South China and East China, with the results shown in Figure 6. The average SST over East China is lower and the SST gradient is greater than those over South China, with a decreasing trend of the former and an increasing trend of the latter (Figures 6a,b). The high-level divergence in both East and South China is decreasing during the landfall from -18 h to +18 h (Figure 6c). However, the high-level flow is dominated by decreasing divergence in South China while that in East China shows convergence (around -1.5×10^{-5} s^{-1}). This means that the upper-level flow is more unfavorable for the maintenance of TCs making landfall over East China. This seems to be consistent with the predominant pre-landfall weakening TCs over East China and intensifying TCs in South China. Moreover, the VWS initially is weaker but increases rapidly over East China while that is moderate over South China (Figure 6d). The westerly vertical shear (UVWS>0) increases during landfall over East China, which implies that a TC would dissipate rapidly after landfall over East China (Figure 6e), consistent with the significant correlation coefficient of 0.22 between LFDR and UVWS300-1000 (Table 2). In contrast, both the deep-layer total VWS and the deep-layer easterly vertical shear (UVWS<0) did not change much during landfall over South China. This implies that the large-scale environmental VWS may not be the key factor affecting TC intensity and post-landfall weakening of TCs over South China.

The mid-tropospheric specific humidity during landfall shows different evolutions over East and South China (Figure 6f). South China is characterized by high mid-tropospheric specific humidity due to the effect of South China Sea summer monsoon compared with East China. Note that the specific humidity increased and decreased the equivalent range over South China and East China, respectively. This explains why the average change in specific humidity for all TC cases is feeble in Table 2. Because of the negative correlation between the mid-tropospheric humidity trend and LFDR (r=-0.19, Table 2), the decreasing humidity over East China contributes to post-landfall weakening while increasing humidity over South China has an opposite effect. The low-level water vapor flux in East China changed from convergence to divergence at 6 h prior to landfall (Figure 6g), indicating that the reduction of water vapor transport into the TC core. Over South China, the low-level water vapor flux maintained a weak convergence of $-0.1\times10^{-6}s^{-1}$. The above results suggest that the faster post-landfall weakening of TCs over East China than over East China was primarily due to lower SST, larger SST gradient, and stronger zonal vertical wind shear, together with the convergence of upper-level flow and the divergence of lower-level water vapor flux.

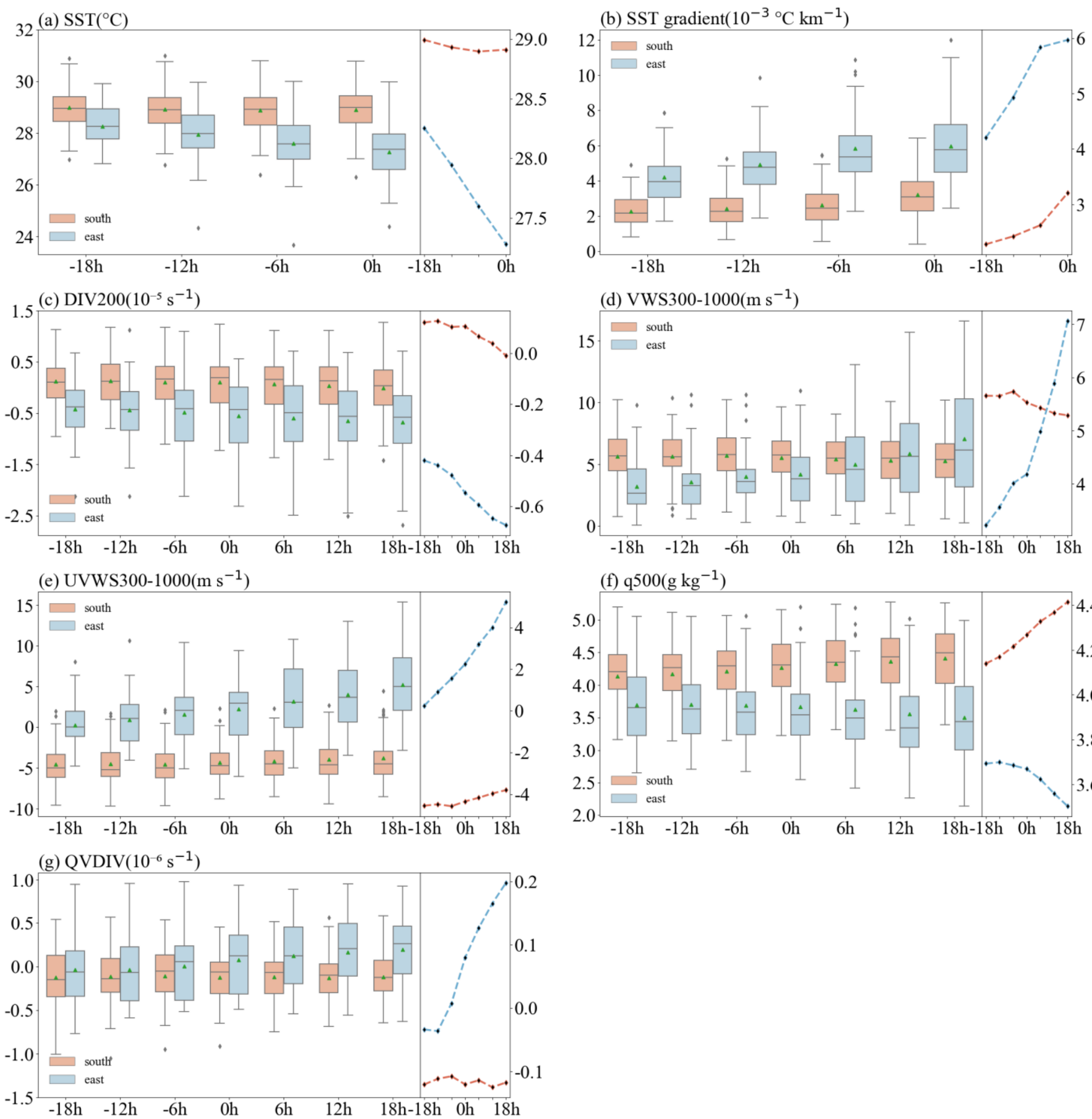

Figure 6. Evolutions of (a) SST (°C), (b) SST gradient (10^{-3} °C km^{-1}), (c) divergence at 200 hPa (10^{-5} s^{-1}), (d) vertical wind shear (m s^{-1}) between 1000 hPa and 300 hPa, (e) zonal vertical wind shear (m s^{-1}) between 1000 hPa and 300 hPa, (f) specific humidity (g kg^{-1}) at 500 hPa, (g) low-level water vapor flux divergence (10^{-6} s^{-1}) between 1000 hPa and 850 hPa during TC landfall over East China (red) and South China (blue). Green dots and horizontal lines represent mean value and median lines, respectively. Right part in each panel represents the evolution of the corresponding mean value of the factor over East China (red) and South China (blue).

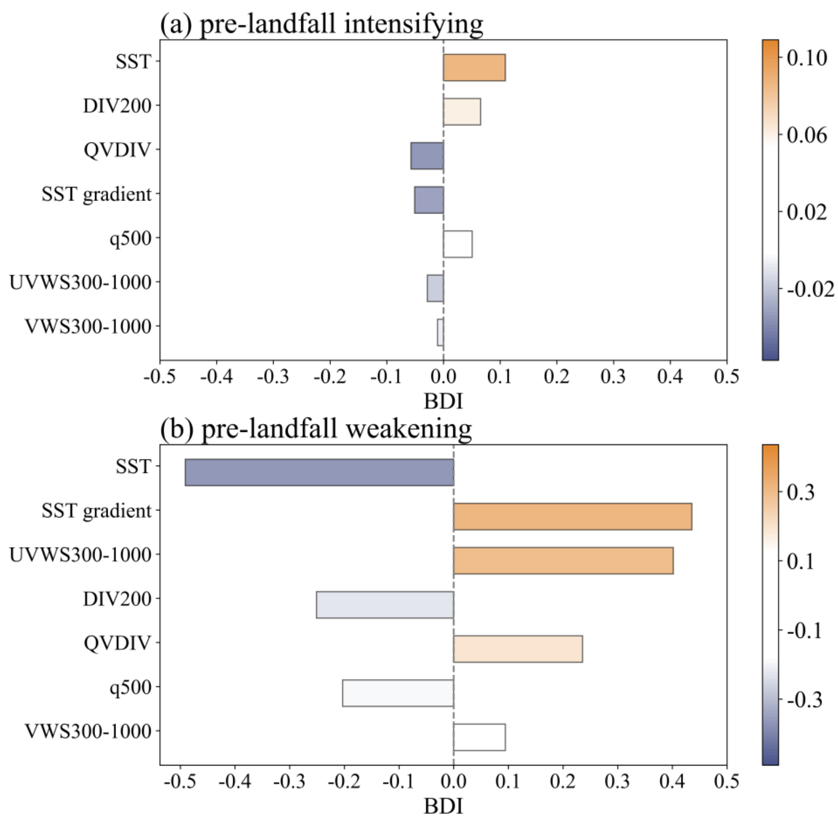

Figure 7. Key factors in (a) intensifying TCs and (b) weakening TCs and their corresponding box difference index (BDI) values prior to landfall. The factors are ordered based on the average values within 18 h prior to landfall.

Factors analyzed above are linked to the ACE prior to and after landfall and can represent their effects of TC intensity change prior to landfall on TC weakening after landfall. This means that the environmental conditions that affect the post-landfall dissipation are mediated by pre-landfall intensity change of TCs. Figure 7 quantifies the relative contributions of key factors to pre-landfall intensifying and weakening TCs using the BDI index, respectively. The results show that the most important factors for distinguishing intensifying TCs from neutral TCs are SST with the BDI value of 0.109. The contributions by other factors are generally secondary with the BDI less than 0.1. As intensifying TCs mostly occurs in South China, the least contribution of UVWS300–1000 (-0.029) and VWS (-0.011) also confirms the above-mentioned conclusion that the large-scale environmental VWS may not be the main factor affecting the pre-landfall weakening of TCs over South China (Figures 6d,e). The q500 also contributes little to LFDR of intensifying TCs over South China, which explains why the specific humidity increases but the TC intensity weakens after landfall in South China. The key factors contributing to the weakening of TCs are SST, SST gradient, and UVWS300–1000 with the BDI values of -0.491, 0.436, and 0.402, respectively. The rests are DIV200 (-0.251), QVDIV (0.236), q500 (-0.203) and VWS300-1000 (0.095). It is worth noting that the contribution by ocean thermodynamic conditions (SST and SST gradient) is very significant, especially for pre-landfall weakening TCs, which is followed by environmental UVWS, consistent with the higher correlation of these factors with LFDR shown in Table 2. In addition, it is clear to see that the BDI values in the intensifying TCs are much smaller than those in the weakening TCs. In other words, environmental factors play a more crucial role in the post-landfall weakening of TCs over East China while the post-landfall dissipation over South China may be controlled by other factors, such as the TC size and structure. As a result, the post-landfall weakening is largely regulated by the intensity change of TCs prior to landfall, which is affected significantly by the coastal ocean thermodynamic and large-scale environmental atmospheric dynamic and thermodynamic conditions.

6. Conclusions

In this study, we first analyzed the intensity change of TCs within 18 h prior to landfall over mainland China during 1979–2018 in the active typhoon season (June–October). The results show that the pre-landfall intensifying TCs usually tend to have small accumulation cyclone energy (ACE_{-18}) and easily maintain larger post-landfall energy (ACE_{+18}) while the weakening TCs with great intensity tend to experience larger energy dissipation after landfall. This indicates that there is a relationship between the pre-landfall intensity change and post-landfall weakening. We also found that the average intensity of intensifying TCs prior to landfall is small and the increasing rate decreases during landfall, while the decreasing rate after landfall is smaller than that of the weakening TCs. The results thus demonstrate that the post-landfall weakening difference of LTCs may result from intensity change prior to landfall.

The distribution of the average change rate in $V_{max}(r_{vmax})$ and LFDR show different regional characteristics over East China and South China. The intensifying TCs are mostly concentrated southeast of Hainan Island, mainly with a southeast-northwest track. The weakening TCs are distributed in both Hainan Province and northern Guangdong to Zhejiang Provinces, moving westward and north-northwestward, respectively. Compared with South China, due to pre-landfall weakening of TCs, TCs making landfall over East China present relatively higher pre-landfall intensity than the intensity at the time of landfall (relative intensity), but possess faster weakening prior to landfall and high LFDR after landfall.

To determine what caused the regional dependence, relevant oceanic and atmospheric environmental factors are statistically analyzed and quantified. Five factors are found to be significantly correlated with LFDR, including SST, SST gradient, environmental VWS between 1000 hPa and 300 hPa (VWS300–1000), zonal environmental VWS between 1000 hPa and 300 hPa (UVWS300–1000), and low-level water vapor flux divergence (QVDIV). This indicates that TCs with greater post-landfall weakening rate usually cross the region with lower SST and greater SST gradient, and are embedded in environment with larger environmental westerly VWS, larger high-level flow convergence and smaller low-level moisture convergence prior to landfall. In addition, decreasing environmental moisture at 500 hPa (q500) are weakly correlated with LFDR, often under 95% significance level.

Results from this study illustrate that the cooling SST and the sharper SST gradient nearshore would promote the high occurrence of rapid weakening prior to landfall because of high BDI values in both intensifying and weakening TCs. For the environmental atmospheric factors, the large deep westerly VWS is also favorable for pre-landfall weakening of TCs, favoring LFDR over mainland China. Nevertheless, above-considered environmental conditions are not key factors leading to pre-landfall intensifying of TCs with very small BDI values over South China and thus play weak role in post-landfall dissipation of intensifying TCs.

The oceanic thermodynamic conditions and the environmental atmospheric conditions over East China show more drastic changes, characterized by smaller and decreasing SST, larger and increasing SST gradient and increasing VWS (particularly, the increasing zonal VWS) in weakening LTCs, resulting in faster energy dissipation after landfall. In addition, upper-tropospheric convergence, decreasing environmental moisture and decreasing convergence of low-level water vapor flux are additional factors conducive to rapid weakening of TCs after landfall over East China. In general, most of these factors changed little over South China but with average values featured with larger SST, small SST gradient, lower VWS, eastern VWS ranging from -2.5m s^{-1} to -5m s^{-1} and wetter environment, all being favorable for pre-landfall weakening TCs over South China to maintain great landfall intensify and weak post-landfall dissipation, and weakly affecting the intensity change of pre-landfall intensifying TCs.

Although we evaluated the relationship between the post-landfall weakening and the pre-landfall TC intensity change of LTCs over mainland China, the conclusions are subject to the limited sample size and the involvements of complex ocean-atmospheric, ocean-land, and land-atmospheric interactions. Note that land surface properties, such as land surface temperature, soil temperature and moisture, vegetation coverage, etc. also affect the post-landfall weakening of TCs (Tuleya and Kurihara, 1978; Tuleya, 1994; Song et al., 2021; Liu et al., 2022; Thomas and Shepherd, 2022). In future studies, the possible effects of land surface properties, including mesoscale terrains (Liu and Wang, 2022), on TC post-landfall weakening can be further examined in combination with large-scale environmental conditions. In addition, it can be also a good topic to introduce the pre-landfall intensity change into the empirical decay model of TCs after landfall (Kaplan and Demaria, 1995; Vickery et al., 2005; Wong et al., 2008; Liu et al., 2021; Liu and Wang, 2022). With improved understanding of key factors affecting TC post-landfall weakening, the forecast accuracy of landfalling TC intensity could be improved.

DATA AVAILABILITY STATEMENT

The STI/CMA TC best track dataset was downloaded from http://tcdata.typhoon.org.cn. The ECMWF Interim data used in this study were downloaded from http://apps.ecmwf.int/datasets/.

AUTHOR CONTRIBUTIONS

YW developed the main idea. WH analyzed the datasets and generated figures. WH and YW wrote the manuscript. LL helped with data pre-processing and provided feedback on the manuscript.

FUNDING

This study has been supported by the National Natural Science Foundation of China under grants 41730960 and 42175011. YW has been supported by the NSF grant AGS-1834300.

Conflict of interest

The authors declare that the research was conducted in the absence of any commercial or financial relationships that could be construed as a potential conflict of interest.

References

Andersen, T. K., and Shepherd, J. M. (2014). A global spatiotemporal analysis of inland tropical cyclone maintenance or intensification. *Int. J. Climatol. 24,* 391–402. doi: 10.1002/joc.3693

Andersen, T. K., Radcliffe, D. E., and Shepherd, J. M. (2013). Quantifying surface energy fluxes in the vicinity of inland-tracking tropical cyclones. *J. Appl. Meteor. Sci. 52,* 2797–2808. doi: 10.1175/jams-d-13-035.1

Bell, G. D., Halpert, M. S., Ropelewski, C. F., Kousky, V. E., Douglas, A. V., Schnell, R. C., et al. (2000). Climate assessment for 1998. *Bull. Am. Meteorol. Soc.* 80, S1 – S48. doi: 10.1175/1520-0477(2000)81[s1:CAF]2.0.CO;2

Bender M. A., Ginis, I., Kurihara, Y. (1993). Numerical simulations of the tropical cyclone-ocean interaction with a high resolution coupled model. *J. Geophys. Res. Atmos.* 98, 23245-23263. doi: 10.1029/93jd02370

Chen, J. L., Tam, C. Y., Cheung, K., Wang, Z., Murakami, H., Lau, N. C., et al. (2021). Changing impacts of tropical cyclones on East and Southeast Asian inland regions in the past and a globally warmed future climate. *Front. Earth Sci. 9, 769005*. doi: 10.3389/feart.2021.769005

Dee, D. P., and Coauthors. (2011). The ERA-Interim reanalysis: configuration and performance of the data assimilation system. *Quart. J. Roy. Meteor. Soc.* 137, 553–597. doi: 10.1002/qj.828

DeMaria, M., DeMaria, R. T., Knaff, J. A., and Molenar, D. (2012). Tropical cyclone lightning and rapid intensity change. *Mon. Weather Rev.* 140, 1828–1842. doi: 10.1175/mwr-d-11-00236.1

Done, J. M., Ge, M., Holland, G., Dima-West, I., Phibbs, S., Saville, G. R., et al. (2020). Modelling global tropical cyclone wind footprints. *Nat. Hazards Earth Syst. Sci.* 20, 67–580. doi: 10.5194/nhes-20-567-2020

Elsberry, R. L., and Tsai, H. C. (2014). Situation-dependent intensity skill metric and intensity spread guidance for western North Pacific tropical cyclones. *Asia-Pac. J. Atmos. Sci.* 50, 297–306. doi: 10.1007/s13143-014-0018-5

Emanuel, K., (2005). Increasing destructiveness of tropical cyclones over the past 30 years. *Nature* 436, 686–688. doi: 10.1038/nature03906

Fei, R., Xu, J., Wang, Y. and Yang, C. (2020). Factors affecting the weakening rate of tropical cyclones over the western North Pacific. *Mon. Weather Rev.* 148, 3693–3712. doi: 10.1175/mwr-d-19-0356.1

Frank, W. M., and Ritchie, E. A. (2001). Effects of vertical wind shear on the intensity and structure of numerically simulated hurricanes. *Mon. Weather Rev.* 129, 2249–2269. doi: 10.1175/1520-0493(2001)129<2249:Eovwso>2.0.Co;2

Franklin, C. N., Holland, G. J. and May, P. T. (2006). Mechanisms for the generation of mesoscale vorticity features in tropical cyclone rainbands. *Mon. Weather Rev.* 134, 2649–2669. doi: 10.1175/mwr3222.1

Fu, B., Peng, M. S., Li, T., and Stevens, D. E. (2012). Developing versus nondeveloping disturbances for tropical cyclone formation. Part II: Western North Pacific. *Mon. Weather Rev.* 140, 1067–1080. doi: 10.1175/2011mwr3618.1

Hu, H., Duan, Y., Wang, Y., and Zhang, X. (2017). Diurnal cycle of rainfall associated with landfalling tropical cyclones in China from rain gauge observations. *J. Appl. Meteor. Climatol.* 56, 2595–2605. doi: 10.1175/jamc-d-16-0335.1

Huang, M., Li, Q., Xu, H., Lou, W., and Lin, N. (2018). Non-stationary statistical modeling of extreme wind speed series with exposure correction. *Wind Struct.* 26, 129–146. doi: 10.12989/was.2018.26.3.129

Ji, Q., Xu, F., Xu, J., Liang, M., Tu, S., and Chen, S. (2019). Large-scale characteristics of landfalling tropical cyclones with abrupt intensity change. *Front Earth Sci.* 13, 808–816. doi: 10.1007/s11707-019-0792-6

Jiang, J. (1989). Analysis of some important characteristics of typhoon No.7 in 1988. *Marine Forecasts* 6, 41–49

Kaplan, J., and DeMaria, M. (1995). A simple empirical model for predicting the decay of tropical cyclone winds after landfall. *J. Appl. Meteor.* 34, 2499–2512. doi: 10.1175/1520-0450(1995)034<2499:asemfp>2.0.co;2

Kaplan, J., and DeMaria, M. (2001). On the decay of tropical cyclone winds after landfall in the New England area. *J. Appl. Meteor.* 40, 280–286. doi: 10.1175/1520-0450(2001)040<0280:Otdotc>2.0.Co;2

Klotzbach, P. J., Steven, S. G. Jr, R. P., and Bell, M. (2018). Continental U.S. hurricane landfall frequency and associated damage: Observations and future risks. *Bull. Am. Meteorol. Soc.* 99, 1359-1276. doi: 10.1175/BAMS-D-17-0184.1

Kruk, M. C., Gibney, E. J., Levinson, D. H., and Squires, M. (2010). A climatology of inland winds from tropical cyclones for the eastern United States. *J. Appl. Meteor. Climatol.* 49, 1538–1547. doi: 10.1175/2010jamc2389.1

Kurihara, Y. M., Bender, M. A., and Ross, R. J. (1993). An initialization scheme of hurricane models by vortex specification. *Mon. Weather Rev.* 121, 2030–2045. doi: 10.1175/1520-0493(1993)121<2030:AISOHM>2.0.CO;2

Li, L., and Chakraborty, P. (2020). Slower decay of landfalling hurricanes in a warming world. *Nature* 587, 230–234. doi: 10.1038/s41586-020-2867-7

Li, R. C. Y., Zhou, W., Shun, C. M., and Lee, T. C. (2017). Change in destructiveness of landfalling tropical cyclones over China in recent decades. *J. Clim.* 30, 3367–3379. doi: 10.1175/jcli-d-16-0258.1

Li, X., Zhan, R., Wang, Y., and Xu, J. (2021). Factors controlling tropical cyclone intensification over the marginal seas of China. *Front. Earth Sci.* 9, 795186. doi: 10.3389/feart.2021.795186

Liang, J., Wu, L., Gu, G., and Liu, Q. (2016). Rapid weakening of Typhoon Chan-Hom (2015) in a monsoon gyre. *Geophys. Res. Lett.* 121, 9508–9520. doi: 10.1002/2016jd025214

Liu, D., Pang, L., and Xie, B. (2009). Typhoon disaster in China: prediction, prevention, and mitigation. *Nat. Hazards* 49, 421–436. doi: 10.1007/s11069-008-9262-2

Liu, L., Wang, Y., Zhan, R., Xu, J., and Duan, Y. (2020). Increasing destructive potential of landfalling tropical cyclones over China. *J. Cim.* 33, 3731–3743. doi: 10.1175/jcli-d-19-0451.1

Liu, L., Wang, Y., and Wang, H. (2021). The performance of three exponential decay models in estimating tropical cyclone intensity change after landfall over China. *Front. Earth Sci.* 9, 792005. doi: 10.3389/feart.2021.792005

Liu, L., and Wang, Y. (2022). A physically based statistical model with the parameterized topographic effect for predicting the weakening of tropical cyclones after landfall over China. *Geophys. Res. Lett.* 49, 1-8. doi: 10.1029/2022gl099630

Liu, Q., Song, J., and Klotzbach, P. J. (2021). Trends in western North Pacific tropical cyclone intensity change before landfall. *Front. Earth Sci.* 9, 780353. doi: 10.3389/feart.2021.780353

Miller, B. I. (1964) A study of the filling of Hurricane Donna (1960) over land. *Mon. Weather Rev.* 92, 389–406. doi: 10.1175/1520-0493(1964)092<0389:asotfo>2.3.CO;2

Ooyama, K. (1969). Numerical simulation of the life cycle of tropical cyclones. *J. Atmos. Sci*. 26, 3-40. doi: 10.1175/1520-0469(1969)026<0003:NSOTLC>2.0.CO;2

Park, D. S. R., Ho, C. H., Kim, J. H., and Kim, H. S. (2011). Strong landfall typhoons in Korea and Japan in a recent decade. *J. Geophys. Res. Atmos.* 116, 1-11. doi: 10.1029/2010jd014801

Powell, M. D., Dodge, P. P., and Black, M. L. (1991). The landfall of Hurricane Hugo in the Carolinas: Surface wind distribution. *Wea. Forecasting* 6, 379–399. doi: 10.1175/1520-0434(1991)006<0379:tlohhi>2.0.co;2

Qian, Y., and Zhang, S. (2013). Cause of the rapid weakening of Typhoon Bebinca (0021) in the South China Sea. *Trop. Cycl. Res. Rev.* 2, 159–168. doi: 10.6057/2013TCRR03.03

Rappaport, E. N., Franklin, J. L., Schumacher, A. B., DeMaria, M., Shay, L. K., and Gibney, E. J. (2010). Tropical cyclone intensity change before U.S. Gulf coast landfall. *Wea. Forecasting* 25, 1380–1396. doi: 10.1175/2010waf2222369.1

Song, J. J., Klotzbach, P. J., Zhao, H., and Duan, Y. H. (2021). Slowdown in the decay of western North Pacific tropical cyclones making landfall on the Asian continent. *Front. Earth Sci.* 9, 749287. doi: 10.3389/feart.2021.749287

Thomas, A. M., and Shepherd, J. M. 2022: A machine-learning based tool for diagnosing inland tropical cyclone maintenance or intensification events. *Front. Earth Sci.* 10, 818671. doi: 10.3389/feart.2022.818671

Trenberth, K. (2005). Uncertainty in hurricanes and global warming. *Science* 308, 1753-1754. doi: 10.1126/science.1112551

Truchelut, R. E., and Staehling, E. M. (2017). An energetic perspective on United States tropical cyclone landfall droughts. *Geophys. Res. Lett.,* 44, 12013–12019. doi: 10.1002/2017gl076071

Tuleya, R. E. (1994). Tropical storm development and decay: Sensitivity to surface boundary conditions. *Mon. Weather Rev.* 122, 291–304. doi: 10.1175/1520-0493(1994)122<0291:tsdads>2.0.CO;2

Tuleya, R. E., and Kurihara, Y. (1978). A numerical simulation of the landfall of tropical cyclones. *J. Atmos. Sci.* 35, 242–257. doi: 10.1175/1520-0469(1978)035<0242:ANSOTL>2.0.CO;2

Tuleya, R. E., Bender, M. A., and Kurihara, Y. (1984). A simulation study of the landfall of tropical cyclones. *Mon. Weather Rev.* 112, 124–136. doi: 10.1175/1520-0493(1984)112<0124:assotl>2.0.CO;2

Vickery, P. J. (2005). Simple empirical models for estimating the increase in the central pressure of tropical cyclones after landfall along the coastline of the United States. *J. Appl. Meteor.* 44, 1807–1826. doi: 10.1175/jam2310.1

Vitart, F. (2009). Impact of the Madden Julian Oscillation on tropical storms and risk of landfall in the ECMWF forecast system. *Geophys. Res. Lett.* 36, 6. doi: 10.1029/2009gl039089

Walsh, K. J. E., McBride, J. L., Klotzbach, P. J., Balachandran, S., Camargo, S. J., Holland, G., et al. (2016). Tropical cyclones and climate change. *WIREs. Climate. Change* 7, 65–89. doi: 10.1002/wcc.371

Wang, W., and YU, J. (2013). Characteristic comparison between the rapid intensification of tropical cyclones in easterly and westerly wind shear over the Northwest Pacific．(in Chinese). *Trans. Atmos. Sci.* 36, 337–345. doi: 10.13878/j.cnki.dqkxxb.2013.03.011

Wang, Y., Rao, Y., Tan, Z., and Schonemann, D. (2015). A statistical analysis of the effects of vertical wind shear on tropical cyclone intensity change over the western North Pacific. *Mon. Weather Rev. 143,* 3434–3453. doi: 10.1175/mwr-d-15-0049.1

Wong, M. L. M., Chan, J. C. L., and Zhou, W. (2008). A simple empirical model for estimating the intensity change of tropical cyclones after landfall along the South China coast. *J. Appl. Meteor. Climatol.* 47, 326–338. doi: 10.1175/2007jamc1633.1

Wood, K. M., and E Ritchie, A. (2015). A definition for rapid weakening of North Atlantic and eastern North Pacific tropical cyclones. *Geophys. Res. Lett.* 42, 10091–10097. doi: 10.1002/2015gl066697

Ying, M., Zhang, W., Yu, H., Lu, X., Feng, J., Fan, Y., et al. (2014). An overview of the China Meteorological Administration tropical cyclone database. *J. Atmos. Oceanic Technol.* 31, 287–301. doi: 10.1175/jtech-d-12-00119.1

Zeng, Z., Wang, Y., and Chen, L. (2010). A statistical analysis of vertical shear effect on tropical cyclone intensity change in the North Atlantic. *Geophys. Res. Lett.* 37, L02802. doi: 10.1029/2009gl041788

Zhang, Q., Wu, L., and Liu, Q. (2009). Tropical cyclone damages in China 1983-2006. *Bull. Am. Meteorol. Soc.* 90, 489-496. doi: 10.1175/2008bams2631.1

Zhang, X., Xiao, Q., and Fitzpatrick, P. J. (2007). The impact of multisatellite data on the initialization and simulation of Hurricane Lili's (2002) rapid weakening phase. *Mon. Weather Rev.* 135, 526–548. doi: 10.1175/mwr3287.1

Zhu, Y. J., Collins, J. M., and Klotzbach, P. J. (2021). Nearshore hurricane intensity change and post-landfall dissipation along the United States Gulf and east coasts. *Geophys. Res. Lett.* 48, 1-10. doi: 10.1029/2021gl094680